Fuel Economy of a Multimode Combustion Engine With Three-Way Catalytic Converter

Sandro P. Nüesch[1]
Powertrain Control Laboratory,
Department of Mechanical Engineering,
University of Michigan,
Ann Arbor, MI 48109
e-mail: snuesch@umich.edu

Anna G. Stefanopoulou
Professor
ASME Fellow
Powertrain Control Laboratory,
Department of Mechanical Engineering,
University of Michigan,
Ann Arbor, MI 48109
e-mail: annastef@umich.edu

Li Jiang
Robert Bosch LLC,
Farmington Hills, MI 48331

Jeff Sterniak
Robert Bosch LLC,
Farmington Hills, MI 48331

Highly diluted, low temperature homogeneous charge compression ignition (HCCI) combustion leads to ultralow levels of engine-out NO_x emissions. A standard drive cycle, however, would require switches between HCCI and spark-ignited (SI) combustion modes. In this paper we quantify the efficiency benefits of such a multimode combustion engine, when emission constraints are to be met with a three-way catalytic converter (TWC). The TWC needs unoccupied oxygen storage sites in order to achieve acceptable performance. The lean exhaust gas during HCCI operation, however, fills the oxygen storage and leads to a drop in NO_x conversion efficiency. If levels of tailpipe NO_x become unacceptable, a mode switch to a fuel rich combustion mode is necessary in order to deplete the oxygen storage and restore TWC efficiency. The resulting lean-rich cycling leads to a penalty in fuel economy. Another form of penalty originates from the lower combustion efficiency during a combustion mode switch itself. In order to evaluate the impact on fuel economy of those penalties, a finite state model for combustion mode switches is combined with a longitudinal vehicle model and a phenomenological TWC model, focused on oxygen storage. The aftertreatment model is calibrated using combustion mode switch experiments from lean HCCI to rich spark-assisted HCCI (SA-HCCI) and back. Fuel and emission maps acquired in steady-state experiments are used. Different depletion strategies are compared in terms of their influence on drive cycle fuel economy and NO_x emissions. It is shown that even an aggressive lean-rich cycling strategy will marginally satisfy the cumulated tailpipe NO_x emission standards under warmed-up conditions. More notably, the cycling leads to substantial fuel penalties that negate most of HCCI's efficiency benefits. [DOI: 10.1115/1.4028885]

1 Introduction

Two primary goals in current automotive industry and legislative focus are an increase in fuel economy and a reduction in emissions. One potential approach toward achieving both targets is advanced combustion technology. HCCI has been an active topic in research for several years [1]. The compression ignition of gasoline leads to low temperature, flameless combustion and an increase in combustion efficiency due to reduced timing losses and improved mixture properties. In addition the chemical reactions producing NO_x emissions are slowed down significantly. To avoid high pressure rise rates the charge requires strong dilution. Therefore the engine is run unthrottled, leading to an additional significant gain in fuel economy due to reduced pumping losses.

The operating regime of HCCI is limited to low and medium loads due to reduced combustion stability and increasing pressure rise rates, respectively. Even though during a standard drive cycle a substantial amount of time is spent within the HCCI operating regime [2] it is not possible to fulfill all the driver demands. A solution is the combination of HCCI with SI combustion in a multimode combustion approach [3]. However, as shown in Refs. [4,5], this requires a large number of combustion mode switches. Due to the inherent differences between SI and HCCI combustion, switches between those two modes are very difficult to control and exhibit a penalty in fuel consumption [6], depending on the applied hardware, actuator strategy, and operating condition. Combustion mode switches are discussed further in Sec. 5.

In order to fulfill the stringent emissions regulations, an aftertreatment system is required. TWCs are the main technology used to control emissions from gasoline engines. However, generally they are not suited for the application in lean-burn direct injection engine systems. TWCs require stoichiometric conditions in order to reduce NO_x, HC, and CO simultaneously. In a lean environment selective catalyst reduction (SCR), lean de-NO_x catalysts or NO_x adsorbers can be used. Nevertheless, as mentioned above due to its low peak temperatures HCCI combustion leads to very low engine-out NO_x emissions. Under lean HCCI conditions the TWC will still be able to convert CO and HC. In addition TWCs have the ability to store a limited amount of O_2 in order to compensate for variations in dilution. If the TWC's oxygen storage capacity (OSC) is sufficiently large, a high NO_x conversion can be sustained for a certain amount of time while running lean HCCI. On the other hand, if the OSC is filled, the TWC needs to be depleted by running the engine rich which translates into a penalty in fuel economy.

The use of TWCs as aftertreatment system is desirable due to their wide distribution and relatively low cost compared to lean-burn aftertreatment systems [7,8]. It is difficult to make a judgment about the benefits of combining HCCI with a TWC. An investigation of the entire system is required, which needs to be based on actual engine data, considers combustion mode switches, and includes the aftertreatment system. Therefore, this paper introduces a methodology to evaluate the impact of a TWC system on fuel economy within a SI–HCCI multimode concept; and to provide insight to the suitability of such a system as an aftertreatment measure enabling high fuel economy and at the same time low emissions on a drive cycle.

In both Refs. [5,9] drive cycle results of an SI–HCCI engine are shown, using simulation-based fuel maps, assuming instantaneous mode switches, and neglecting emissions. An investigation of the tradeoff between emissions and fuel economy during various mode switches from SI to SA-HCCI was conducted in Ref. [10]. The analysis is based on experiments without drive cycle

[1]Corresponding author.

Contributed by the Dynamic Systems Division of ASME for publication in the Journal of Dynamic Systems, Measurement, and Control. Manuscript received March 28, 2014; final manuscript received October 14, 2014; published online December 10, 2014. Assoc. Editor: Gregory Shaver.

Table 1 Engine specifications

Number of cylinders	4
Displacement	2.0 L
Compression ratio	11.7:1
Bore/stroke	86 mm/86 mm
Con. rod length	145.5 mm
High/low cam lift	10 mm/4 mm

simulations. The experimental data were used for calibrating the aftertreatment models used in this full system simulation study. Similar issues about the effectiveness of a new technology are studied in Ref. [11], where the use full vehicle simulations and static engine maps to evaluate a different advanced combustion mode, namely reactivity controlled compressed ignition, in terms of fuel economy and engine-out emissions has been pursued. Similarly, this paper applies the longitudinal vehicle model explained and validated in Ref. [4] to show drive cycle fuel economy results. The methodology is extended by including steady-state emissions maps based on experiments with the multimode engine, shown in Sec. 2. Mode switch experiments, explained in Sec. 3, are used to parameterize and validate a simple TWC and oxygen storage model in Sec. 4. The combustion mode switch model, shown in Ref. [2], is extended in Sec. 5 by accounting for rich SI combustion and emissions during the mode switches. In Sec. 6, three different oxygen storage depletion strategies are introduced and their impact on drive cycle fuel economy and emissions are discussed in Sec. 7.

2 Hardware and Experimental Setup

2.1 Hardware. The engine used in this paper is a 2.0 L I4 multimode combustion engine with a stock turbocharger, specifications listed in Table 1. Due to increased compression ratio, two-step cam profile switching, electric cam phasing for recompression, and stronger reciprocating components it is possible to run naturally aspirated (NA) HCCI besides the traditional SI mode. For control during nominal operation the aftertreatment system consists of three Emitec prototype TWC substrates with the first two substrates housed together in one can and the third packaged as an underfloor catalyst. The close coupled TWC substrates are based on palladium (Pd) and palladium/rhodium (Pd/Rh), and the underfloor TWC is based on palladium/rhodium (Pd/Rh). The two catalysts use a generous cerium dioxide–zirconia dioxide (CeO_2–ZrO_2) oxygen storage. The hardware configuration is sketched in Fig. 1. The system is operated with two oxygen sensors (or λ-sensors). A wide-range sensor is located in front of the first catalyst and a switching-type sensor in between the two catalysts. The hardware is discussed in more detail in Ref. [10].

2.2 Experimental Setup. The sensors used for the experiments are also shown in Fig. 1. In addition to the wide-range λ-sensor in front of the first TWC two additional ones were placed in between the two and after the second catalyst, respectively. Furthermore, the NO_x emissions were measured using Cambustion CLD500 fast-NO_x analyzers with a response time $T_{10–90}$ of 10 ms. The space velocity was approximately 13,000 h^{-1}.

SI–HCCI combustion mode switches require sophisticated control strategies. At the time of the experiments the two-stage cam profile system and the control strategy were under development. Ideally a full switch would have been carried out during the experiments, including switches from low to high lift cams. Instead, using variable valve timing and a stoichiometric or rich air–fuel ratio (AFR), an extension strategy was tested with a switch to a mode described as SA-HCCI combustion. In this mode SI combustion conditions are approached, nevertheless they consist of both flame propagation and some autoignition. Further information about spark-assisted compression ignition can be found in Refs. [12,13]. More details about the experimental setup and results are described in Ref. [10].

3 Experiments

3.1 Steady-State

3.1.1 Brake Specific Fuel Consumption (BSFC) and Emission Maps. In steady-state experiments maps of the multimode combustion engine were acquired, consisting of BSFC, relative AFR λ, and engine-out emissions over brake mean effective pressure (BMEP) and engine speed ω_e, depicted in Fig. 2. In the following the maps are referred to as $NO_{x,SI}$ (BMEP, ω_e) and $NO_{x,HCCI}$ (BMEP, ω_e). As can be seen the use of HCCI leads to benefits in BSFC of more than 20% at low loads while it approaches SI values toward higher loads, it operates also much closer to stoichiometry. Significant reduction in NO_x emissions can be noticed as well, especially in the lower half of the operating regime. The HCCI regime overlaps with a region in which SI can be operated using external exhaust gas recirculation (eEGR). This strategy already results in a substantial decrease in NO_x emissions. Nevertheless HCCI reduces those additionally by more than 95%.

Note that only NA HCCI conditions are considered. Even though the engine is turbocharged the HCCI exhaust enthalpy of the engine considered was too low to build significant boost in the stock turbocharger. The advanced combustion regime can be extended by using multi-injection, multi-ignition (MIMI) strategies [14], SA-HCCI [15,16], or boosted HCCI [17].

3.1.2 Conversion Efficiency. The conversion efficiency of the TWCs was measured at different dilutions and combustion modes, shown in Fig. 3. The engine was operated at 1800 RPM and between 1.6 bar and 3.1 bar BMEP. Under lean AFR conditions the TWC is ineffective in converting NO_x, leading to equal pre- and postcat NO_x values. However, due to measurement errors the postcat concentration may appear slightly larger than the precat one, leading to negative conversion efficiencies. Therefore, for such cases zero conversion was assumed. As can be seen the static NO_x conversion of the TWC is independent of the combustion modes. The impact of the low exhaust gas temperature of HCCI on the TWC temperature is discussed in Ref. [3]. However, based on Ref. [4] during an FTP-75 driving cycle, stays in the HCCI region are generally shorter than 100 engine cycles ($=6$ s at 2000 RPM). Therefore, since stays in HCCI mode are too short to have a strong effect on TWC temperature, and engine cold start is not considered in this work, it is assumed that the temperature always remains well above light-off. Consequently, the fit for conversion efficiency is only a function of relative AFR λ while other factors, such as temperature and chemical composition, are neglected

$$\eta_{NO_x}(\lambda) = 99.9087 \frac{1 + \exp^{-789.6}}{1 + \exp^{783.5 \cdot \lambda - 789.6}} \tag{1}$$

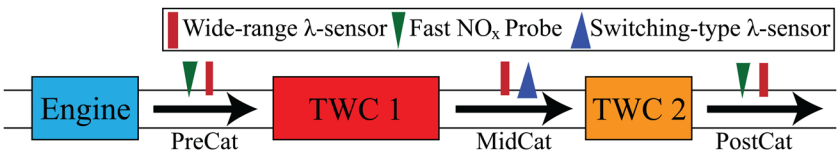

Fig. 1 Hardware setup for aftertreatment experiments and control

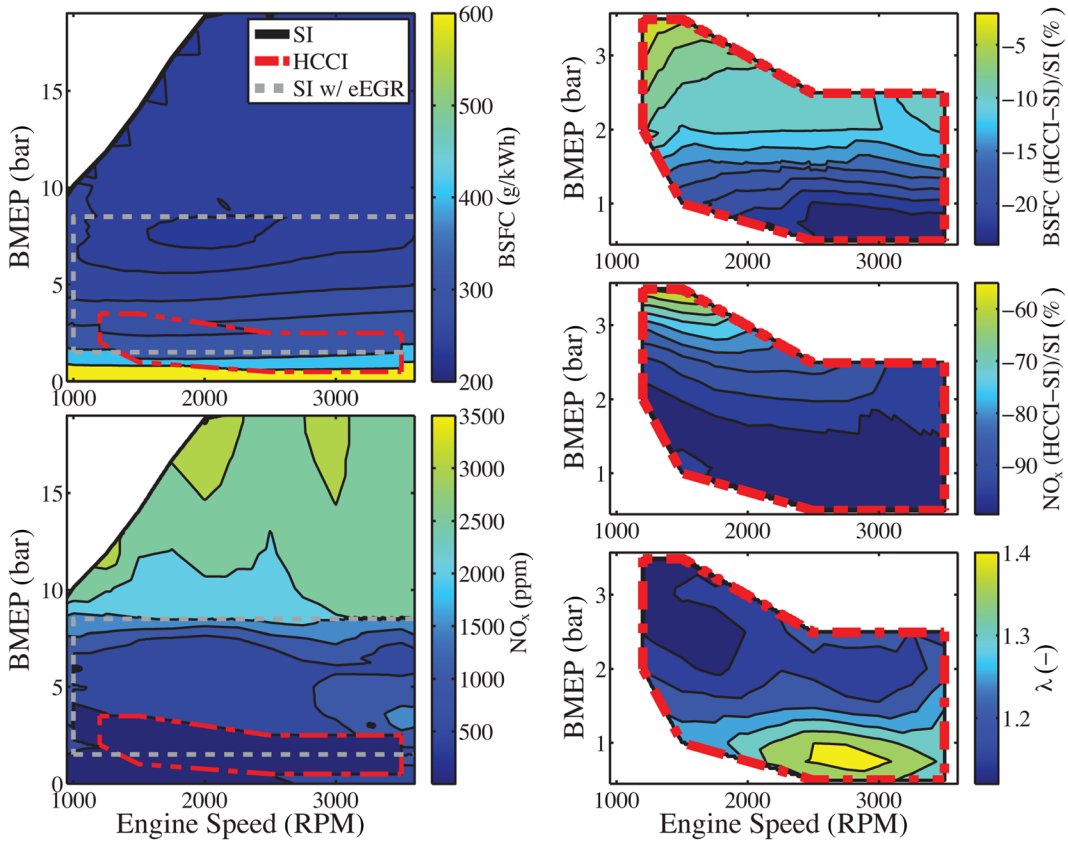

Fig. 2 Maps of the multimode combustion engine based on experiments. Lean HCCI with low NO_x (dashed-dotted), SI combined with eEGR (dotted). Left: On top BSFC map and below engine-out NO_x map. Right: Top and center show improvements in BSFC and NO_x within the operating regime of HCCI compared to SI, respectively. Bottom: Map of relative AFR λ.

Using the same experimental data a very basic approximation for the NO_x at rich conditions was found, shown in Fig. 4. In reality engine-out emissions during rich operation depend on many different factors. In strong simplification a function $h_{rich}(\lambda)$ is assumed to decrease the steady-state NO_x value proportionally with λ. During the transient experiments and the simulations $\lambda = 0.9$ was the most rich condition that occurred.

3.2 Transient Mode Switch. Combustion mode switch experiments were conducted in Ref. [10] at different levels of dilution. In this paper, the data is used in order to characterize the two TWCs and their OSC. The combustion mode was switched between lean HCCI at $\lambda = \{1.06, 1.16, 1.34\}$ and rich SA-HCCI at $\lambda = \{0.9, 0.98\}$. The engine speed was kept constant at 1800 RPM and the load moved between 2 bar and 3 bar BMEP. During the combustion mode switches, actuators settings such as intake and exhaust valve timing, injected fuel mass, and start of injection were linearly moved between the steady-state settings during 1 s.

It must be noted that, even though this is a representative mode switch strategy, there is potential to reduce the duration, fuel consumption, and NO_x emissions during the mode switch beyond what we consider. However, a game-changing, but highly unlikely, strategy of mode-switching would have to be found under rich conditions at very low engine-out NO_x to actually alter the conclusion. In addition, as mentioned above, a complete mode switch to SI would involve switching the lift of the cams.

Experimental results of one particular run are shown in Fig. 5. As can be seen the oxygen storage delays the breakthrough of λ after the mode switches. As soon as the storage is full and λ_{post} switches to lean the conversion efficiency drops to zero and the NO_x postcat is equal to NO_x precat. During the mode switches spikes in NO_x levels occur beyond their steady-steady values. The reason is the mode switch control strategy, that favors NO_x production during the switch by allowing larger fuel amounts together with lean AFRs. Postcat NO_x continuously decreases to 0 ppm as the oxygen storage is being depleted and the TWC's NO_x conversion efficiency gradually increases. In addition it is possible that the increased oxygen partial pressure during the lean phase lead to filling of storage sites that are difficult to reach under

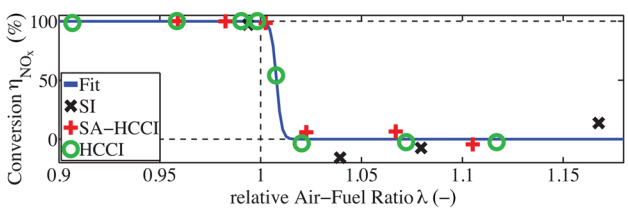

Fig. 3 TWC NO_x conversion efficiency measurements at 1800 RPM and fit (solid). SI (cross), SACI (plus), and HCCI (dotted).

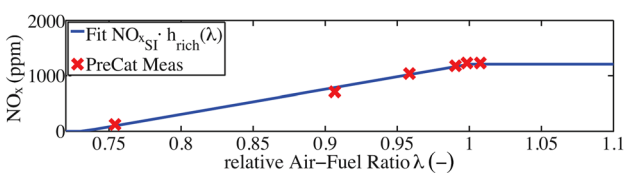

Fig. 4 Steady-state NO_x precat measurements in SI mode at 1800 RPM (cross) and linear fit (solid) over AFR

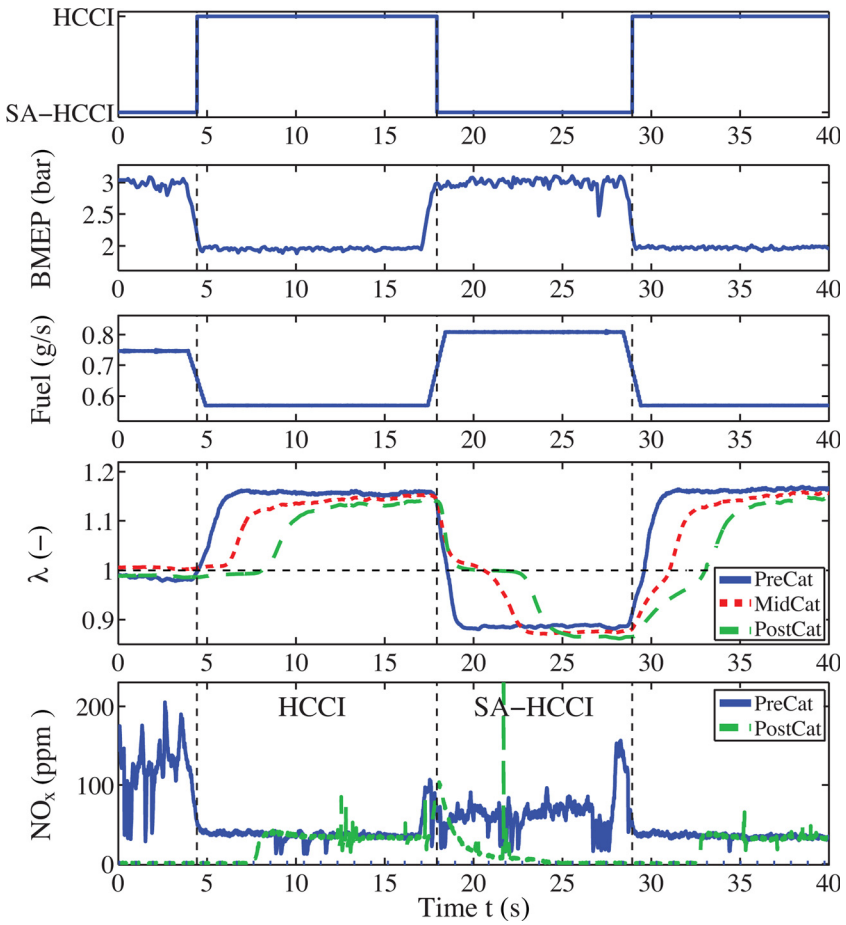

Fig. 5 Combustion mode switch experiment between rich SA-HCCI ($\lambda = 0.9$) and lean HCCI ($\lambda = 1.16$). Top: Combustion mode based on EVC position. The center of the linear cam phasing of 1 s represents the mode switch (dashed vertical). Second and third: BMEP and fuel mass flow command, respectively. Fourth: Precat AFR measurements (solid), midcat (dashed), and postcat (dotted). Bottom: NO_x measurements precat (solid) and postcat (dotted).

conditions closer to stoichiometry [10]. Comparing these experimental results to examples published in literature (e.g., Refs. [18,19]), a difference is apparent after the switch from SA-HCCI to HCCI at $t = 30$ s. After the precat AFR is changed from rich to lean, mid- and post-cat λ values are expected to show a fast response until they reach stoichiometry. Instead they exhibit a slow response. One possible explanation for this behavior might be the storage of hydrocarbons on the TWC during extensive rich operation. The hydrocarbons might get desorbed during the succeeding lean phase, leading to a rich postcat λ.

4 Oxygen Storage

4.1 Model. Modeling the chemical reactions occurring in a catalyst accurately requires detailed kinematic models [20–22]. Nevertheless several approaches can be found in literature introducing simplifications to the system to make it more feasible for control-purposes. Those simplified models are either phenomenological and oxygen storage-dominated [23,24] or based on reduced chemical relationships [18,25,26]. They try to estimate the relative oxygen storage level, one of the most important states for aftertreatment control. In this paper the approach shown in Refs. [27] and [28] is applied. In an effort to obtain an initial estimate of the fuel penalties due to emission constraints, the simple oxygen storage model was applied at all loads and speeds, extrapolating the behavior of the local conditions used for tuning the model.

In the following, the implementation of the model in this paper is briefly repeated. A block diagram of the model is shown in Fig. 6. The relative oxygen storage level Θ is the only state, temperature dynamics are neglected because the periods within the HCCI region are very short so there is not much time for cooling down the TWC. Inputs are air mass flow $\dot{m}_a$, incoming NO_x concentration, and relative AFR λ_{in}. Outputs are outgoing NO_x concentration and relative AFR λ_{out}.

The function $\rho(\Theta, \lambda_{in})$ regulates how fast the OSC can be filled and lies between 0 and 1. In short, an empty storage can be filled faster than a full one, vice versa for depletion. The functions f_L and f_R represent the fraction of oxygen being adsorbed from and released to the feed gas, respectively,

$$f_L(\Theta) = \frac{1 - e^{p_L \Theta}}{e^{p_L} - 1} + 1 \tag{2}$$

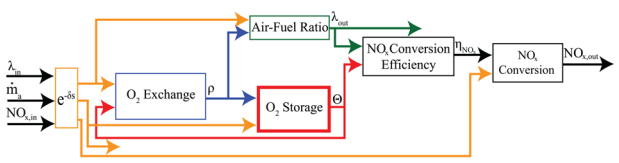

Fig. 6 Block diagram of the TWC model, introduced in Ref. [27]

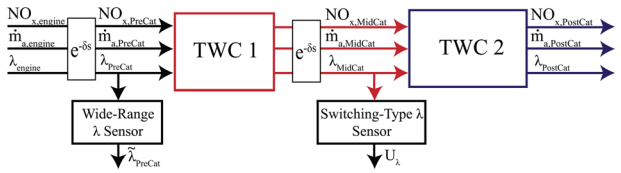

Fig. 7 Block diagram of the system with the two TWCs and the two sensors

$$f_R(\Theta) = \frac{e^{-p_R\Theta} - 1}{e^{-p_R} - 1} \tag{3}$$

$$\rho(\Theta, \lambda_{in}) = \begin{cases} f_L(\Theta) & \lambda_{in} \geq 1 \\ f_R(\Theta) & \lambda_{in} < 1 \end{cases} \tag{4}$$

Parameters p_L and p_R determine the shape of those functions. They were chosen so that the simulated behavior of pre- and post-cat λ matches the one in the experiments.

According to Ref. [27] an increase in effective OSC, represented as parameter C, can be observed with an increase in $\dot{m}_a$. This approach was also feasible to describe the experiments in this paper. Instead of varying C, $\dot{m}_a$ was saturated at parameter $\dot{m}_{a,sat}$, leading to the same effect. The variable $\dot{m}'_a$ is used in the Θ state equation. From mass balance output λ_{out} can be easily derived in Eq. (7)

Table 2 OSC model and estimation parameters

Storage capacities	C_1	0.7	C_2	0.4	$\tilde{C}_1$	0.7
Adsorption	$p_{L,1}$	6.6	$p_{L,2}$	4.5		
Release	$p_{R,1}$	8.1	$p_{R,2}$	6.5		
Saturation	$\dot{m}_{a,sat}$	8.2 g/s	$\tilde{m}_{a,sat}$	10 g/s		
PI	k_p	0.08	T_i	25 s		

$$\dot{m}'_a = \min\{\dot{m}_a, \dot{m}_{a,sat}\} \tag{5}$$

$$\Theta = \begin{cases} \frac{0.23}{C}\left(1 - \frac{1}{\lambda_{in}}\right) \cdot \dot{m}'_a \cdot \rho & 0 \leq \Theta \leq 1 \\ 0 & \text{else} \end{cases} \tag{6}$$

$$\lambda_{out} = \lambda_{in} - \rho(\lambda_{in} - 1) \tag{7}$$

Figure 7 shows the block diagram of the mathematical model of the aftertreatment system with the two connected TWC blocks. The transport delays δ, occurring between engine and TWC 1 as well as between TWC 1 and TWC 2, depend on ω_e and are chosen to be half of an engine cycle to match the experimental data. Also shown are the two sensors measuring λ_{PreCat} and λ_{MidCat}, resulting in $\tilde{\lambda}_{PreCat}$ and U_λ, respectively.

4.2 Validation. The seven unknown parameters C_1, C_2, $p_{L,1}$, $p_{L,2}$, $p_{R,1}$, $p_{R,2}$, and $\dot{m}_{a,sat}$ were found by matching the model to the transient mode switch experiments at the different conditions for λ. The results are shown in Table 2. The model was validated with additional experimental data sets at the same operating conditions. Figure 8 shows the comparison of the model to one of these experiments. Steady-state map values for BSFC and engine-out λ and NO_x at same speed/load conditions were used as inputs. Durations and behavior of λ during filling and depletion of the OSCs are very comparable. It can also be seen that both the steady-state NO_x values match as well as the instant where the OSC is full and the conversion efficiency drops. As expected by the model

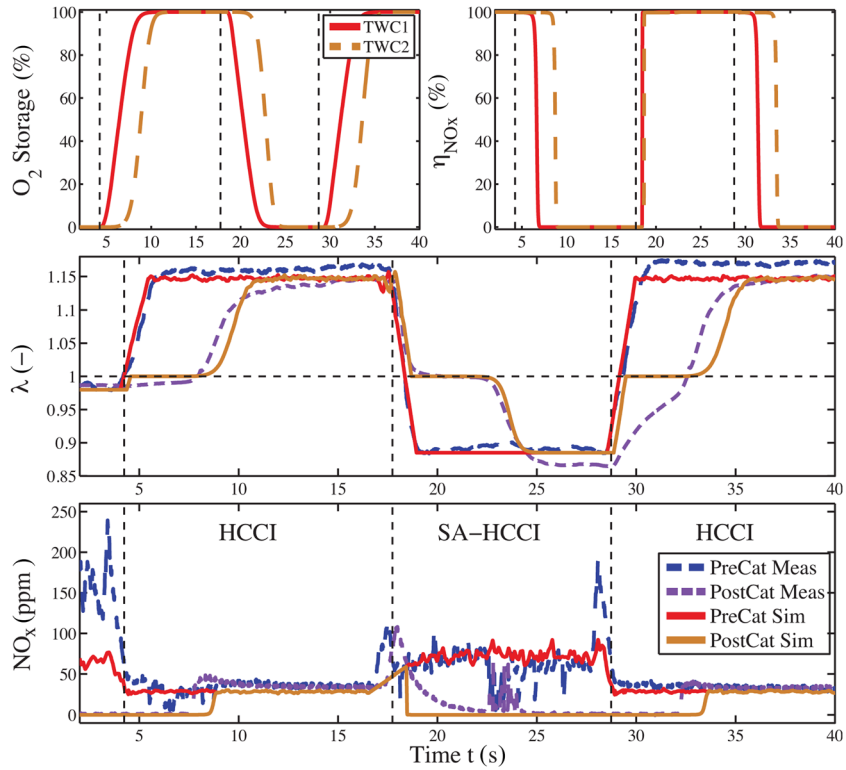

Fig. 8 Validation of the aftertreatment model with a different experimental data set at same conditions as in Fig. 5. Top: Left and right plots of the OSC level and NO_x conversion efficiency, respectively, for the two TWCs. Center and bottom: Relative AFR λ and NO_x, respectively. Precat and postcat measurements (dashed dark gray and dotted medium gray, respectively). Precat and postcat simulation (solid medium gray and solid light gray, respectively).

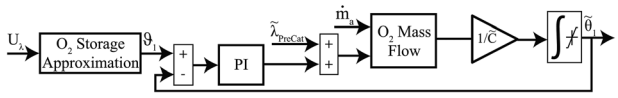

Fig. 9 Block diagram of the OSC estimator

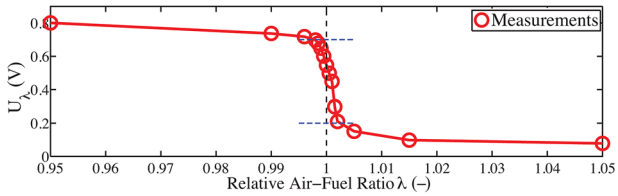

Fig. 10 Switching-type sensor voltage—AFR characteristic

construction, this simplified model is not able to reproduce the roll-off in postcat NO_x at $t = 18$ s but shows an instantaneous drop to zero. In addition since steady-state maps are used the NO_x spikes during rich-to-lean transitions are not recreated. Another disagreement can be seen at $t = 30$ s when $\lambda_{PostCat}$ steps to stoichiometry immediately instead of following the slow response of the measurement.

This model is only parameterized and validated for medium loads and speeds. Due to the saturation of air mass flow at $\dot{m}_{a,sat} = 8.2\text{g/s}$ this model is likely to overestimate the OSC and therefore the time required for its depletion at higher loads. However, for this work it only required to approximate the oxygen storage dynamics within the HCCI load range and for that purpose this model is considered to be accurate enough.

4.3 Estimation. It is not necessary to solely rely on the model in order to detect a deplete or full oxygen storage. The very accurate switching-type sensor, located in between the two catalysts, provides feedback as soon as the AFR switches from lean to rich and vice versa. A model-based closed-loop estimation approach shown in Refs. [29] and [30] is adapted and integrated. The structure of the estimator is shown in Fig. 9.

The wide-range oxygen sensor in front of the first catalyst is modeled as a first-order system with noise. In reality these sensors are also prone to biases which are neglected here

$$\tilde{\lambda}_{PreCat} = \frac{1}{1+\tau s}\lambda_{PreCat} + \text{Noise} \tag{8}$$

Figure 10 shows the λ-voltage characteristic of the implemented switching-type sensor. The following equation, shown by Ref. [31], translates the sensors voltage output U_λ into an oxygen storage estimation ϑ_1 by simply interpolating the signal in a narrow range around stoichiometry

$$\vartheta_1 = \begin{cases} 1 & U_\lambda < 0.2\text{V} \\ 1-(U_\lambda - 0.2)/0.5 & 0.2\text{V} \le U_\lambda \le 0.7\text{V} \\ 0 & 0.7\text{V} < U_\lambda \end{cases} \tag{9}$$

A correctional input $\Delta\lambda$ is derived by comparing ϑ_1 with the estimated $\tilde{\Theta}_1$ whenever λ_{MidCat} is close to stoichiometry. The integrator of the PI controller resets as soon as the gas composition deviates from stoichiometry

$$\Delta\lambda = \begin{cases} PI(\vartheta_1 - \tilde{\Theta}_1) & 0.2\text{V} \le U_\lambda \le 0.7\text{V} \\ 0 & \text{else} \end{cases} \tag{10}$$

As already shown above the same expression for the saturation of the air mass flow was used, leading to the state equation for $\tilde{\Theta}_1$

$$\dot{\tilde{m}}'_a = \min\{\dot{m}_a, \dot{\tilde{m}}_{a,sat}\} \tag{11}$$

$$\dot{\tilde{\Theta}}_1 = \frac{0.23 \cdot \dot{\tilde{m}}'_a}{\tilde{C}} \cdot \left(1 - \frac{1}{\tilde{\lambda}_{PreCat} + \Delta\lambda}\right) \tag{12}$$

Table 2 also lists the parameters for the estimator $\tilde{C}_1$ and $\dot{\tilde{m}}_{a,sat}$. This model is almost equal to the one used as plant. As can be seen, its parameters differ slightly from the ones of the model to include some model uncertainty. For a more realistic plant, a parameter adaptation scheme as described in Ref. [30] is required to lead to good performance over the entire operating range.

5 Combustion Mode Switch Model

5.1 Combustion Mode Switch. Above it was mentioned that controlling combustion mode switches between SI and HCCI is challenging. The reason being the large difference in their operating conditions. Conditions in SI mode are close to stoichiometry with positive valve overlap and a small amount of residual gas while HCCI mode corresponds to lean combustion with negative valve overlap and a significant amount of residuals. Experimental studies [6,32,33] show the presence of an unstable region with high cyclic variability between SI and HCCI combustion. Such conditions often lead to poor combustion efficiency, and a more complex control problem. Depending on utilized hardware, different control strategies are discussed in literature. In Ref. [34], fully flexible valve actuators are used due to their great range of manipulation. An alternative hardware setup is used by Ref. [35], in which a control strategy is based on a two-step cam profile switching system, due to its lower cost as compared to the fully flexible actuation.

Different control strategies lead to different engine-out emissions, AFR, and fuel penalties during mode switches, which need to be accounted for in drive cycle simulations. If instantaneous mode switches are assumed the two BSFC maps are simply used and the fuel penalties are completely neglected, as in Ref. [36]. Here, the penalization is implemented by using the finite state machine introduced in Ref. [2]. In this paper the model, depicted in Fig. 11, was extended to account for the influence of the aftertreatment system. Assumptions used for fuel penalties d_i during the mode switch are shown in Fig. 11. For more details, it is referred to Ref. [2]. The fuel beneficial region is denoted $R(k) \in \{\text{SI, HCCI}\}$. In addition to the previously published model, the binary control input r is used to command a mode switch to the rich SI mode. This leads to the modified region $\hat{R}(k) \in \{\text{SI, HCCI, rich SI}\}$

$$\hat{R}(k) = \begin{cases} \text{rich SI} & r(k-1) = \text{true} \\ R(k) & \text{else} \end{cases} \tag{13}$$

5.2 AFR. All the finite states are divided based on their dilution and labeled as $L(k) \in \{\text{Stoich, Lean, Rich}\}$. For $L(k) = \text{Stoich}$ the engine-out AFR is assumed to be exactly stoichiometric without any deviations due to inaccuracies or AFR control. The value of λ in case $L(k) = \text{Rich}$ is a control input. More fuel leads to a faster depletion of the OSC but also higher fuel penalty. Here $\lambda = 0.9$ was chosen. For $L(k) = \text{Lean}$ the map output λ_{HCCI} from Fig. 2 is used. Therefore as long as $L(k)$ remains constant λ_{engine} is calculated as follows:

$$\lambda_{engine} = \begin{cases} 1 & L(k) = \text{Stoich} \\ 0.9 & L(k) = \text{Rich} \\ \lambda_{HCCI}(\text{BMEP}, \omega_e) & L(k) = \text{Lean} \end{cases} \tag{14}$$

Changes from $L(k) = \text{Stoich}$ to Rich or vice versa are assumed to be linear interpolations between the steady-state values during

three engine cycles. Of course in reality the dilution during the combustion mode switches will strongly depend on the applied control strategy.

5.3 NO_x. While $L(k) \in \{\text{Stoich, Lean}\}$ the engine-out $NO_{x,engine}$ is equal to the respective map values $NO_{x,SI}$ and $NO_{x,HCCI}$. For $L(k) = \text{Rich}$ the SI map output is modified using the linear approximation function h_{rich}, as shown in Fig. 4

$$NO_{x,engine} = \begin{cases} NO_{x,SI}(BMEP, \omega_e) & L(k) = \text{Stoich} \\ NO_{x,SI}(BMEP, \omega_e) \cdot h_{rich}(\lambda_{engine}) & L(k) = \text{Rich} \\ NO_{x,HCCI}(BMEP, \omega_e) & L(k) = \text{Lean} \end{cases} \tag{15}$$

If $L(k)$ changes from Stoich to Rich or vice versa the NO_x map is changed instantaneously. This is a strong assumption since, depending on the control strategy and engine operating conditions, spikes in NO_x occur, as seen in Fig. 5 at $t = 28$ s during the transition from SA-HCCI to HCCI.

6 Depletion Strategies

In order to maximize fuel economy it is necessary to remain in the HCCI combustion mode for as long as possible while minimizing the total mode switch fuel penalty. On the other hand, running lean HCCI eventually fills up the OSC and stops the conversion of NO_x. Therefore, the OSC must be depleted when returning to SI combustion by running the engine rich in order to avoid break through of the unacceptably high engine-out NO_x during SI operation. Of course running rich SI leads to an additional penalization of fuel economy.

However, catalyst oxygen storage depletion might already be necessary before the operating regime of HCCI is left. To begin with, even though the NO_x emissions in HCCI are very low, summed up over an entire drive cycle they might be too high to

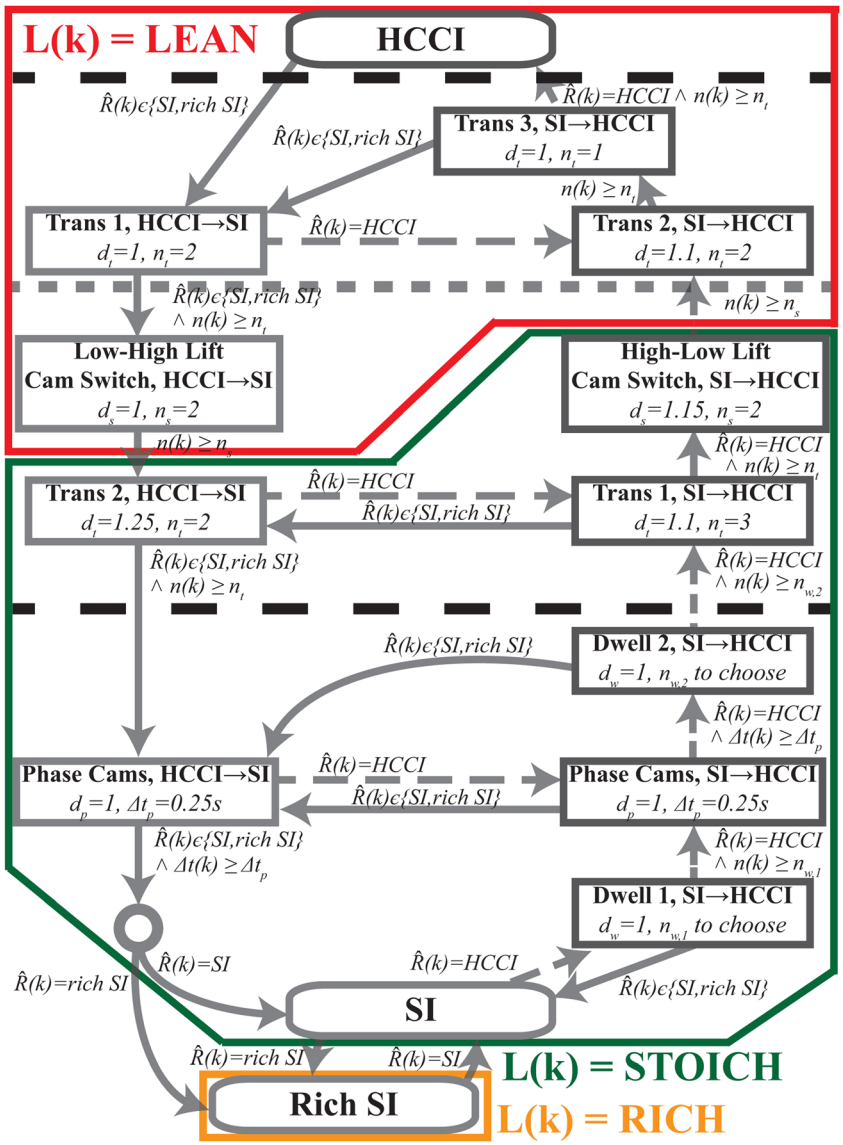

Fig. 11 Finite state model of the combustion mode switch between SI and HCCI as shown in Ref. [2]. Rich SI combustion state was added. Depending on the control input *r*, $\hat{R}(k)$ denotes the currently BSFC-beneficial region or rich SI. The combustion modes were divided based on their dilution into $L(k) \in \{\text{Stoich, Lean, Rich}\}$. The number of cycles and the time since entering the current mode are denoted as states $n(k)$ and $\Delta t(k)$, respectively. The assumed parameters are fuel penalties d_i and durations n_i and Δt_i for each finite state i.

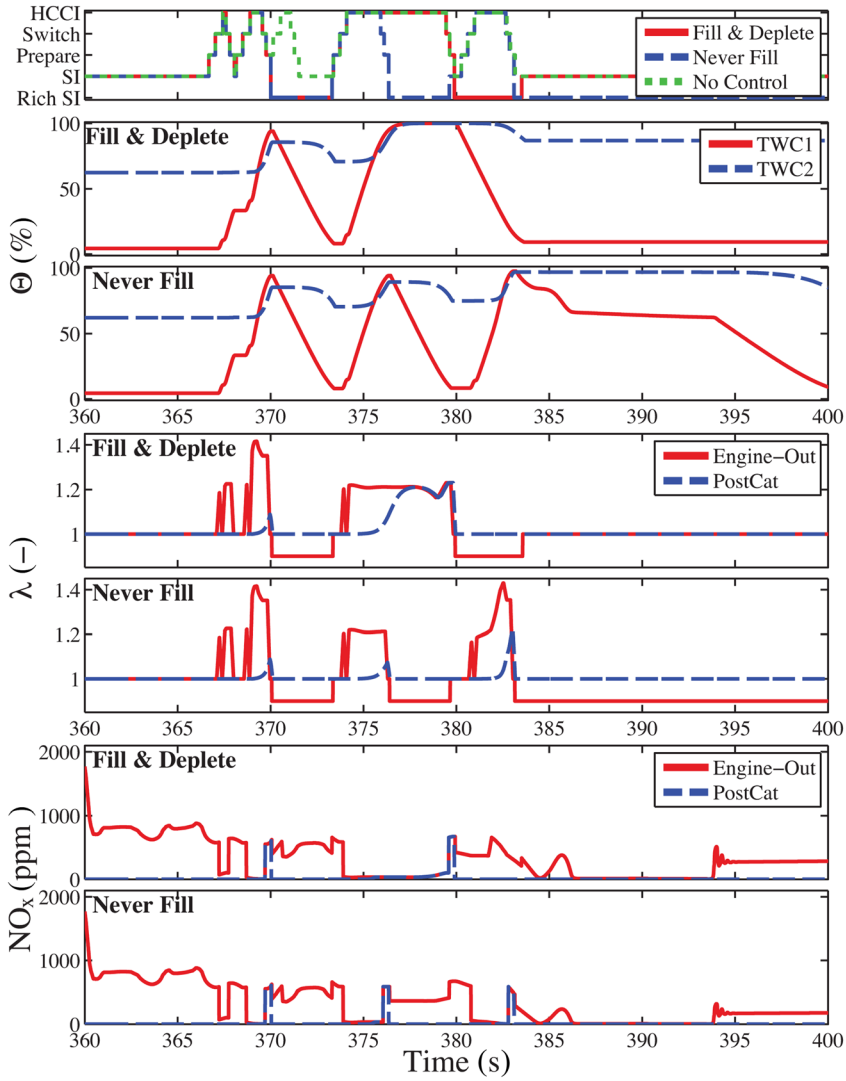

Fig. 12 Comparison of depletion strategies Fill & Deplete and Never Fill at an example time interval during a drive cycle. Top: Currently active combustion mode. Intermediate modes from Fig. 11 summarized as Prepare and Switch. No Control (dotted), Never Fill (dashed), and Fill & Deplete strategy (solid). Second and third: Comparison of OSC trajectories for the two strategies, TWC 1 (solid) and TWC 2 (dashed). Fourth and fifth: λ. Sixth and seventh. NO_x engine-out (solid) and tailpipe (dashed).

fulfill very restrictive emissions requirements without aftertreatment. Furthermore, if NO_x spikes occur during HCCI to SI mode switches it is necessary to have some OSC remaining in order to maintain conversion efficiency during the switch. For those reasons the aftertreatment system could not only lead to a fuel economy penalty due to depletion but also because of premature cancellation of stays in HCCI.

In the following, three strategies are investigated in terms of fuel economy and NO_x emissions. Figure 12 depicts a comparison of the strategies at an illustrative drive cycle situation.

6.1 Strategy: No Control of Oxygen Storage. The first strategy completely ignores NO_x emissions. There are no premature mode switches out of HCCI and also no OSC depletions. Therefore, the control value remains $r(k) = \text{false}$. This is an oversimplified strategy, used in the case when NO_x levels during HCCI operation as well as mode switches are low enough to fulfill the emissions requirements without exhaust aftertreatment. This will lead to the maximum drive cycle fuel economy. In reality, similar to a case after fuel cut-off events, some OSC depletion is always necessary in order to ensure high catalytic conversion, even in stoichiometric SI mode.

6.2 Strategy: Fill and Deplete After Mode Switch. The second strategy is a compromise between fuel economy and emissions. When the engine operates in HCCI mode, $M(k) = \text{HCCI}$, the following conditions apply to the control value:

$$r(k) = \begin{cases} \text{true} & \tilde{\Theta}_1 > 0.9 \text{ and } R(k) = \text{SI} \\ \text{false} & \text{else} \end{cases} \tag{16}$$

Therefore, a switch to rich SI is only demanded if the OSC is estimated as full and the HCCI regime is left. The engine remains in depletion mode, $M(k) = \text{rich SI}$, until the OSC is empty

$$r(k) = \begin{cases} \text{false} & \tilde{\Theta}_1 = 0 \\ \text{true} & \text{else} \end{cases} \tag{17}$$

As soon as this is the case, a mode switch back to HCCI again becomes a possibility. Otherwise, if $M(k) \notin \{\text{rich SI, HCCI}\}$, the control remains constant, $r(k) = r(k-1)$.

This strategy leads to a fuel penalty due to the rich operation. However, it should not substantially reduce the total time spent in HCCI.

6.3 Strategy: Never Fill. The third strategy prohibits to completely fill the OSC, e.g., to ensure conversion of potential engine-out NO_x spikes during mode switches. In any mode, except for $M(k) \neq$ rich SI, a depletion is demanded as soon as the OSC is full

$$r(k) = \begin{cases} \text{true} & \tilde{\Theta}_1 > 0.9 \\ \text{false} & \text{else} \end{cases} \tag{18}$$

Then the operation remains in $M(k) =$ rich SI, until the storage is detected as depleted

$$r(k) = \begin{cases} \text{false} & \tilde{\Theta}_1 = 0 \\ \text{true} & \text{else} \end{cases} \tag{19}$$

This strategy leads to the largest penalization in fuel economy due to the cancellation of stays in HCCI and the more frequent depletion phases. On the other hand, it should result in the lowest emissions.

7 Drive Cycle Results

The strategies introduced above were applied in the federal test procedure (FTP-75) drive cycle simulation and compared to the SI-only case. Only the second and third phases of the FTP-75 were used since the temperature dynamics during cold start were neglected. The results are plotted in Fig. 13.

It can be seen that the penalties due to the mode switches as well as the depletion have significant impact on fuel economy. Even if instantaneous mode switches are assumed, it is apparent that the potential fuel economy benefits from using HCCI are negated entirely as soon as lean-rich cycling and succeeding OSC depletion phases are required.

As expected, the SI-only case leads to the highest engine-out NO_x. However, overall the difference between the strategies is relatively small, since SI is in any case the predominant mode. This might change if NO_x spikes during mode switches need to be considered. Those would especially increase the average engine-out NO_x for the never fill strategy, due to the high number of mode switches.

For tailpipe NO_x, the SI-only case leads to the lowest results by orders of magnitude due to the assumption of exactly stoichiometric combustion and perfect TWC conversion. The "No Control" strategy without any oxygen storage control leads to the highest NO_x emissions. Applying the mode switch fuel penalty leads to a reduction in NO_x since time in HCCI is subtracted by the durations of the mode switches. Certainly this depends on the conditions assumed during the mode switch. The use of either of the two depletion strategies leads to a significant reduction in tailpipe NO_x emissions.

Shown is also the LEV II SULEV limit of 20 mg/mi average tailpipe NO_x emission during the FTP-75 drive cycle. As can be seen all the results, except for the SI-only case, are either very close or over the limit.

The quantitative results need to be treated with caution. As mentioned a large number of assumptions and simplifications were applied in the process. The oxygen storage model is very simple, neglects temperature, composition, nonequilibrium effects, etc., and was only locally parameterized. If operating conditions are found under which the OSC could be depleted at lower fuel cost, the penalty of lean-rich cycling would decrease. In addition, the performance of HCCI could be more fuel beneficial than stated, if its operating regime can be enlarged and its engine-out emissions at higher loads reduced. This would extend the duration

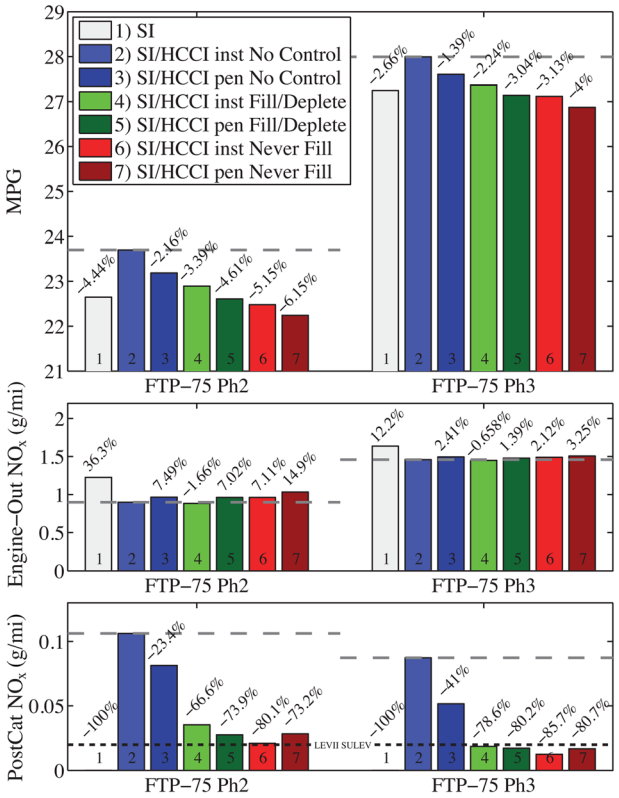

Fig. 13 Drive cycle simulation results. Top: Fuel economy. Center: Average engine-out NO_x. Bottom: Average tailpipe NO_x. Three different oxygen storage depletion strategies compared for instantaneous and penalized mode switches. For the penalties, the assumptions shown in Fig. 11 were applied. Instantaneous case applying the strategy without control was used as baseline (dashed gray). Results are compared to LEV II SULEV limit 20 mg/mi (dotted black). Left and right, results are shown for the second and third phases of the FTP-75, respectively.

per stay in HCCI mode. Also, if it is possible to conduct a combustion mode switch in a shorter amount of time and with lower fuel and NO_x penalties than assumed here, a higher number of mode switches would have a less harmful effect on overall fuel economy.

However, it has to be expected that in a more thorough analysis of the entire FTP-75 drive cycle the LEVII SULEV limits would be exceeded due to the following reasons: First, transient effects and possible NO_x spikes have been neglected, leading generally to an increase in engine-out NO_x. Second, the first phase of the FTP-75 drive cycle includes warm-up of the TWC. In general during this phase the largest portion of tailpipe NO_x is produced. Therefore, additional NO_x emissions originating from cold-start need to be accounted for. Third, exact stoichiometry and perfect NO_x conversion are assumed in SI mode, which are simplifications as well. Together with the large penalty in fuel economy it can be concluded that a TWC aftertreatment system in a SI–HCCI multimode context is not suited for low emissions and requires an engine operation that reduces fuel efficiency.

8 Conclusion

A longitudinal vehicle model, a combustion mode switch state machine, and a phenomenological, oxygen storage dominated TWC model were combined in order to evaluate the fuel economy and NO_x emissions of a SI–HCCI multimode combustion engine on drive cycle level. The impact of two fuel penalties was investigated. The first one reflects directly the combustion conditions during the mode switches. The second one arises from the

requirement of depleting the catalyst's oxygen storage by running the engine rich. Three illustrative aftertreatment strategies were compared, each targeting a different trade-off between fuel economy and emissions. It is shown that subsequent depletion of the TWC negates the fuel economy benefits gained during efficient HCCI operation. In addition low emissions standards for NO_x were not robustly secured. Despite the large number of assumptions and simplifying models this methodology is easily extendable. In further work a more detailed TWC model can be implemented in order to investigate effects of temperature and cold-start. SI–HCCI mode switch experiments at different operating conditions allow a more general characterization of fuel penalties, NO_x spikes and AFR behavior. Passive SCR systems, in combination with TWCs with reduced OSC, might be a successful alternative. Nevertheless, they require a similar investigation of the entire system in order to estimate their feasibility in terms of ammonia storage capacity. After all, the emissions problem can be circumvented if it is focused on stoichiometric combustion modes such as stoichiometric, SA-HCCI. SA-HCCI extends the operating regime of advanced combustion to higher loads compared to lean (NA) HCCI. However, the benefits in efficiency are reduced. Currently, SA-HCCI is not available at lower loads since spark loses control authority. Not much work has been done on stoichiometric HCCI without spark-assist so far.

Acknowledgment

The authors wish to thank Dr. Stanislav Bohac and Patrick Gorzelic for helpful discussions on three-way catalysts and combustion mode switches. This material is based upon work supported by the Department of Energy [National Energy Technology Laboratory] under Award Number DE-EE0003533. This work is performed as a part of the ACCESS project consortium (Robert Bosch, LLC, AVL Inc., Emitec Inc., Stanford University, and University of Michigan) under the direction of PI Hakan Yilmaz and Co-PI Oliver Miersch-Wiemers, Robert Bosch, LLC.

References

[1] Thring, R., 1989, "Homogeneous Charge Compression Ignition (HCCI) Engines," SAE Paper No. 892068.
[2] Nüesch, S., Hellström, E., Li, J., and Stefanopoulou, A., 2014, "Mode Switches Among SI, SACI, and HCCI Combustion and Their Influence on Drive Cycle Fuel Economy," American Control Conference, Portland, OR, June 4–6, pp. 849–854.
[3] Kulzer, A., Hathout, J.-P., Sauer, C., Karrelmeyer, R., Fischer, W., and Christ, A., 2007, "Multi-Mode Combustion Strategies With CAI for a GDI Engine," SAE Paper No. 2007-01-0214.
[4] Nüesch, S., Hellström, E., Li, J., and Stefanopoulou, A., 2013, "Influence of Transitions Between SI and HCCI Combustion on Driving Cycle Fuel Consumption," European Control Conference, Zurich, Switzerland, July 17–19, pp. 1976–1981.
[5] Ortiz-Soto, E., Assanis, D., and Babajimopoulos, A., 2012, "A Comprehensive Engine to Drive-Cycle Modelling Framework for the Fuel Economy Assessment of Advanced Engine and Combustion Technologies," Int. J. Engine Res., **13**(3), pp. 287–304.
[6] Kakuya, H., Yamaoka, S., Kumano, K., and Sato, S., 2008, "Investigation of a SI–HCCI Combustion Switching Control Method in a Multi–Cylinder Gasoline Engine," SAE Paper No. 2008-01-0792.
[7] Posada, F., Bandivadekar, A., and German, J., 2013, "Estimated Cost of Emission Control Technologies for Light-Duty Vehicles. Part 1—Gasoline," SAE Paper No. 2013-01-0534.
[8] Posada, F., Bandivadekar, A., and German, J., 2013, "Estimated Cost of Emission Control Technologies for Light-Duty Vehicles. Part 2—Diesel," SAE Paper No. 2013-01-0539.
[9] Wheeler, J., Polovina, D., Frasinel, V., Miersch-Wiemers, O., Mond, A., Sterniak, J., and Yilmaz, H., 2013, "Design of a 4-Cylinder GTDI Engine With Part-Load HCCI Capability," SAE Paper No. 2013-01-0287.
[10] Chen, Y., Sima, V., Lin, W., Sterniak, J., and Bohac, S., 2014, "Fuel Efficiency and NO_x Reduction From Multi-Mode Combustion With Three-Way Catalysts," ASME ICED Fall Technical Conference, Columbus, IN, Oct. 19–22.
[11] Gao, Z., Curran, S., Daw, C., and Wagner, R., 2013, "Light-Duty Drive Cycle Simulations of Diesel Engine-Out Exhaust Properties for an RCCI-Enabled Vehicle," 8th U.S. National Combustion Meeting, University of Utah, May 19–23, Paper No. 070IC-0220.
[12] Lavoie, G., Martz, J., Wooldridge, M., and Assanis, D., 2010, "A Multi-Mode Combustion Diagram for Spark Assisted Compression Ignition," Combust. Flame, **157**(6), pp. 1106–1110.
[13] Manofsky, D., Vavra, J., Assanis, D., and Babjimopoulou, A., 2011, "Bridging the Gap Between HCCI and SI: Spark-Assisted Compression Ignition," SAE Paper No. 2011-01-1179.
[14] Yun, H., Wermuth, N., and Najt, P., 2009, "Development of Robust Gasoline HCCI Idle Operation Using Multiple Injection and Multiple Ignition (MIMI) Strategy," SAE Paper No. 2009-01-0499.
[15] Kalian, N., Zhao, H., and Yang, C., 2009, "Effects of Spark-Assistance on Controlled Auto-Ignition Combustion at Different Injection Timings in a Multicylinder Direct-Injection Gasoline Engine," Int. J. Engine Res., **10**(3), pp. 133–148.
[16] Johansson, T., Johansson, B., and Tunestål, P., 2009, "HCCI Operating Range in a Turbo-Charged Multi Cylinder Engine With VVT and Spray-Guided DI," SAE Paper No. 2009-01-0494.
[17] Olsson, J.-O., Tunestål, P., and Johansson, B., 2004, "Boosting for High Load HCCI," SAE Paper No. 2004-01-0940.
[18] Tsinoglou, D., Koltsakis, G., and Peyton Jones, J., 2002, "Oxygen Storage Modeling in Three-Way Catalytic Converters," Ind. Eng. Chem. Res., **41**(5), pp. 1152–1165.
[19] Peyton Jones, J., 2003, "Modeling Combined Catalyst Oxygen Storage and Reversible Deactivation Dynamics for Improved Emissions Prediction," SAE Paper No. 2003-01-0999.
[20] Aimard, F., Li, S., and Sorine, M., 1996, "Mathematical Modeling of Automotive Three-Way Catalytic Converters With Oxygen Storage Capacity," Control Eng. Pract., **4**(8), pp. 1119–1124.
[21] Ohsawa, K., Baba, N., and Kojima, S., 1998, "Numerical Prediction of Transient Conversion Characteristics in a Three-Way Catalytic Converter," SAE Paper No. 982556.
[22] Kumar, P., Gu, T., Grigoriadis, K., Franchek, M., and Balakotaiah, V., 2014, "Spatio-Temporal Dynamics of Oxygen Storage and Release in a Three-Way Catalytic Converter," Chem. Eng. Sci., **111**, pp. 180–190.
[23] Peyton Jones, J., Roberts, J., and Bernard, P., 2000, "A Simplified Model for the Dynamics of a Three-Way Catalytic Converter," SAE Paper No. 2000-01-0652.
[24] Muske, K., and Peyton Jones, J., 2004, "Estimating the Oxygen Storage Level of a Three-Way Automotive Catalyst," American Control Conference, Boston, MA, June 30–July 2, Vol. 5, pp. 4060–4065.
[25] Kiwitz, P., Onder, C., and Guzzella, L., 2012, "Control-Oriented Modeling of a Three-Way Catalytic Converter With Observation of the Relative Oxygen Level Profile," J. Process Control, **22**(6), pp. 984–994.
[26] Kumar, P., Makki, I., Kerns, J., Grigoriadis, K., Franchek, M., and Balakotaiah, V., 2012, "A Low-Dimensional Model for Describing the Oxygen Storage Capacity and Transient Behavior of a Three-Way Catalytic Converter," Chem. Eng. Sci., **73**, pp. 373–387.
[27] Brandt, E., Wang, Y., and Grizzle, J., 2000, "Dynamic Modeling of a Three-Way Catalyst for SI Engine Exhaust Emission Control," IEEE Trans. Control Syst. Technol., **8**(5), pp. 767–776.
[28] Fiengo, G., Grizzle, J., Cook, J., and Karnik, A., 2005, "Duel-UEGO Active Catalyst Control for Emissions Reduction: Design and Experimental Validation," IEEE Trans. Control Syst. Technol., **13**(5), pp. 722–736.
[29] Shafai, E., Roduner, C., and Geering, H., 1996, "Indirect Adaptive Control of a Three-Way Catalyst," SAE Paper No. 961038.
[30] Ammann, M., Geering, H., Onder, C., Roduner, C., and Shafai, E., 2000, "Adaptive Control of a Three-Way Catalytic Converter," American Control Conference, Chicago, IL, June 28–30, Vol. 3, pp. 1561–1566.
[31] Guzzella, L., and Onder, C., 2010, *Introduction to Modeling and Control of Internal Combustion Engine Systems*, Springer, Berlin, Germany.
[32] Zhang, Y., Xie, H., Zhou, N., Chen, T., and Zhao, H., 2007, "Study of SI–HCCI–SI Transition on a Port Fuel Injection Engine Equipped With 4VVAS," SAE Paper No. 2007-01-0199.
[33] Matsuda, T., Wada, H., Kono, T., Nakamura, T., and Urushihara, T., 2008, "A Study of Gasoline-Fueled HCCI Engine Mode Changes From SI Combustion to HCCI Combustion," SAE Paper No. 2008-01-0050.
[34] Roelle, J., Shaver, M., and Gerdes, J., 2004, "Tackling the Transition: A Multi-Mode Combustion Model of SI and HCCI for Mode Transition Control," Proceedings of the ASME Dynamic Systems and Control Division, ASME Paper No. IMECE2004-62188.
[35] Yang, X., and Zhu, G., 2012, "SI and HCCI Combustion Mode Transition Control of an HCCI Capable Engine," IEEE Trans. Control Syst. Technol., **21**(5), pp. 1558–1569.
[36] Lawler, B., Ortiz-Soto, E., Gupta, R., Peng, H., and Filipe, Z., 2011, "Hybrid Electric Vehicle Powertrain and Control Strategy Optimization to Maximize the Synergy With a Gasoline HCCI Engine," SAE Paper No. 2011-01-0888.